

# Constr aints on Physical P roperties of $z \approx 6$ G alaxies U sing Cosm ological H ydrodynam ic S imulations

K ristian F inlator, Rom eeld ave, Ben jam in D .O ppenheimer  
D epartment of A stronomy, U niversity of A rizona, Tucson, A Z 85721

18 February 2019

## A B S T R A C T

We introduce Spoc, a new code for constraining the physical properties of observed galaxies through a Bayesian likelihood comparison with galaxies drawn from simulations. Spoc inputs an object's photometric and outputs probability distributions of stellar mass, star formation rate (SFR), age, metallicity, dust extinction, and redshift (if none is given) for that galaxy. We apply Spoc, employing model galaxies drawn from CDM cosmological hydrodynamic simulations, to Abel 2218 KESR ( $z = 6.7$ ) and five other  $z > 5.5$  galaxies for which published rest-frame ultraviolet and optical measurements are available. We compare the outcome of using our simulated galaxies' star formation histories (SFHs) versus using simple one-parameter SFHs such as constant, exponentially-decaying, and rising (a new form we introduce motivated by typical SFHs seen in our simulated galaxies). We show that simulated galaxies match these observations at least as well as simple SFHs, with similar favored values obtained for the intrinsic physical parameters such as stellar mass and SFR, but with substantially smaller uncertainties. This shows that the existence of galaxies at  $z > 5.5$  with properties as observed is straightforwardly accommodated within current hierarchical structure formation scenarios. Our Spoc-derived photometric redshifts agree well with the available spectroscopic redshifts. We examine several models for galactic outflows and reddening, and show that most inferred physical properties are insensitive to these choices. Hence Spoc provides a robust tool for optimally utilizing hydrodynamic simulations (or any model that predicts galaxy SFHs) to constrain the physical properties of individual galaxies having only photometric data.

**K ey w ords:** galaxies: formation, galaxies: evolution, galaxies: high-redshift, cosmology: theory, methods: numerical

## 1 IN T R O D U C T I O N

Over the last few years, observations of galaxies at  $z \approx 6$  have opened up a new window into the reionization epoch, turning it into the latest frontier both for observational and theoretical studies of galaxy formation. Planned (Gonzalez-Serrano et al. 2005) and existing wide-area narrowband searches for  $z \approx 5.5$  objects such as the Subaru Deep Field (Ajiki et al. 2006; Shimakawa et al. 2006), the Large Area Lyman-Alpha Survey (Rhoads & Malhotra 2001; Malhotra & Rhoads 2004), the Chandra Deep Field-South (Wang et al. 2005; Malhotra et al. 2005), and the Hubble Ultra Deep Field (Malhotra et al. 2005) are now combining with Lyman-alpha dropout searches (Dickinson et al. 2004; Bouwens et al. 2004a,b; Mobasher et al. 2005; Bouwens et al. 2006), targeted searches near lensing caustics in galaxy clusters (Kneib et al. 2004; Hu et al. 2002) and occasionally serendipity (Stem et al. 2005) to

uncover star-forming galaxies from the reionization epoch in significant numbers<sup>1</sup>.

Two questions are immediately raised by this new stream of observations: (1) What are the physical properties of these objects?; and (2) What constraints do they place on current models of galaxy formation? The latter question has been addressed in a number of recent papers, taking the canonical approach of producing "simulated observations" that may be directly compared to data (Somerville et al. 2001; Idzi et al. 2004; Night et al. 2005; Finlator et al. 2006; Dave et al. 2006). These studies generically show that current simulations are broadly consistent with available observations, though there are hints of discrepancies such as an excess of predicted galaxies at both the bright and faint ends

<sup>1</sup> A listing of spectroscopically-confirmed  $z > 5$  galaxies can be found in Berger et al. 2006.

## 2 F in lator, D ave, O ppenheim er

of the luminosity function. However, these bulk comparisons shed only indirect light on the nature of any discrepancies.

Answering the first question is more desirable, particularly on an individual galaxy basis, but is also more challenging since it requires a detailed understanding of the relationship between the observed light and the underlying physical properties. If high-quality spectra are available, such inferences become relatively reliable, but unfortunately these distant systems are typically too faint for that to be feasible. Given the broad success of simulations in reproducing current observations of high- $z$  galaxies, it is worthwhile to examine how such models might inform our understanding of the relationship between observed broad-band light and physical properties.

Clearly, the amount of physical insight that can be inferred depends on the quantity and quality of the available data. For some high- $z$  galaxies, only narrow-band photometry and rest-frame ultraviolet (UV) spectroscopy are available (e.g., Cuby et al. 2003; Kodaira et al. 2003; Rhoads et al. 2003; Kurk et al. 2004; Rhoads et al. 2004; Stern et al. 2005; Westra et al. 2005). For others, an emission-line measurement and 1/3 rest-UV broad bands are available (e.g., Nagao et al. 2004; Stanway et al. 2004a,b; Nagao et al. 2005; Stiavelli et al. 2005; Hu et al. 2004). Studies employing the Lyman dropout technique in the optical must further contend with the possible presence of low-redshift interlopers (Dickinson et al. 2004; Bouwens et al. 2004a,b) and large uncertainties from dust extinction. Nevertheless, some interesting constraints can be placed on the underlying physical properties of the sources from solely rest-UV data (Dory et al. 2005; Gwyn & Hartwick 2005).

With the addition of rest-frame optical data, e.g. from Spitzer's Infrared Array Camera (IRAC), it becomes possible to obtain simultaneous constraints for the stellar mass, SFR, dust extinction, and redshift using spectral energy distribution (SED) fitting techniques (Egami et al. 2005; Chary, Stern & Eisenhardt 2005; Eyles et al. 2005; Mobasher et al. 2005; Yan et al. 2005; Schaefer & Pello 2005; Dunlop et al. 2006). The uncertainties inherent in such analyses primarily stem from a poor constraint on the age of the galaxy's stellar population, because the relationship between age and the strength of the telltale Balmer break depends on the form of the assumed star formation history (SFH) (e.g., Papovich et al. 2001; Shapley et al. 2005). This age uncertainty propagates via a host of degeneracies into increased uncertainties in the inferred mass, SFR, metallicity, and dust extinction, if no priors are assumed on these quantities. Additional uncertainties arise from the unknown form of the appropriate template SED (e.g. Schaefer & Pello 2005) and the treatment of stellar evolution assumed by the chosen population synthesis models (see e.g. Maraston et al. 2006). Still, SED fitting offers the most promising approach for determining the physical properties of large numbers of high- $z$  galaxies.

Cosmological hydrodynamic simulations offer the possibility, in principle, of significantly improving SED fitting constraints. This is primarily because the range of SFHs that typically occur in the simulations is a small subset of the range that is physically plausible, ensuring tighter age constraints. Furthermore, as we will show here there is little dependence of the SFH for a given mass galaxy on poorly-constrained physical processes such as outflows.

The physical reason for this is that the dominant growth mode for high redshift galaxies is smooth, cold accretion (Keres et al. 2005), which is primarily tied to the slowly and smoothly growing galactic potential. Hence while some details of galaxy formation remain poorly understood, the overall form of high-redshift galaxy SFHs appears to be fairly generic.

Given this, how can one employ simulations to improve constraints on SED fitting? One can view a numerical simulation as producing a Monte Carlo sampling of parameter space such that the frequency with which a given set of physical parameters ought to occur is proportional to the number of galaxies in the simulation that are characterized by that set of parameters. In essence, numerically-simulated galaxies provide "implicit priors" for SED fitting, i.e. solutions that are *a priori* weighted more heavily because they occur more frequently. The underlying assumption is that simulated galaxy SFHs represent those occurring in nature; indeed, testing this assumption is one of the key goals of this process.

In this paper we introduce Spoc (Simulated Photometry-derived Observational Constraints), a flexible tool that uses Bayesian formalism to constrain the physical properties of observed galaxies based on photometric measurements. We show that it gives results that are consistent with those from more traditional one-parameter SFHs, but with significantly tighter constraints. We go on to apply Spoc to a sample of  $z > 5.5$  galaxies from the literature having rest-frame optical photometry, and show that the simulated galaxies fit observations at least as well as one-parameter SFHs. Since there is no guarantee that simulations produce galaxy SFHs that actually occur in nature, the fact that good fits can be obtained is a non-trivial success of the model, and shows that the existence of such galaxies is straightforwardly accommodated in current hierarchical structure formation scenarios.

Section 2 introduces Spoc, detailing our Bayesian formalism and discussing systematic uncertainties. Section 3 presents the simulations and the one-parameter models that will be used as the template library for Spoc. Section 4 discusses what drives the inferred physical properties in the context of our simulations, and shows that Spoc accurately recovers the physical properties of simulated galaxies. Section 5 explores the best-fit parameters of one observed reionization-epoch galaxy in detail, and compares with results from traditional one-parameter SFH models. Section 6 repeats the previous comparison for a larger set of observed galaxies, highlighting the variety of interesting results that Spoc obtains. Finally, in Section 7 we present our conclusions.

## 2 M E T H O D O L O G Y O F Spoc

Here we summarize the Bayesian statistical method employed in Spoc. Pedagogical explanations of SED fitting techniques have been presented elsewhere (Bentz 2000; Kauffmann et al. 2003), so we refer the reader there for more detailed discussion of those aspects.

## 2.1 The Spoc Equation

Our goal is to constrain the stellar mass, SFR, mean stellar metallicity, age, dust extinction, and redshift ( $M^*$ ,  $M_{\star}$ ,  $z$ ,  $t$ ,  $A_V$ , and  $z$ , respectively) based on available measurements  $D$ . According to Bayes' Theorem, the probability  $p$  that the measurements  $D$  correspond to a galaxy with the intrinsic physical parameters  $\hat{M}^*; \hat{M}_{\star}; \hat{z}; \hat{t}; \hat{A}_V; \hat{z}$  (where a hat indicates a particular value of a parameter) is given by

$$p(\hat{D}) / p(\hat{D})p(D|\hat{D}): \quad (1)$$

The prior  $p(\hat{D})$  indicates the relative a priori probability that a randomly selected galaxy has this particular combination of parameters, and the likelihood  $p(D|\hat{D})$  indicates the probability of obtaining the measurements  $D$  for a galaxy characterized by the parameters  $\hat{D}$ ; for a given model galaxy and data set  $D$  this is assumed to be proportional to  $e^{-\frac{1}{2}(\hat{D}-D)^2}$ . Any information regarding the expected distributions of physical properties of the observable galaxies (such as the stellar mass function) or relationships between these properties (such as a mass-metallicity relation) can be taken into account via a contribution to the prior, and will generally give rise to more precise and possibly more accurate constraints.

In this work, we assume uniform priors on  $z$  and  $A_V$ , and we do not assume any dependence between  $A_V$  and the other intrinsic physical properties. We introduce an additional prior  $p(\text{sim})$  to account for any other priors. For example, when matching observed galaxies against model galaxies derived from the outputs of two cosmological simulations that span different comoving volumes,  $p(\text{sim})$  represents the ratio of the simulation volumes. After several applications of the product rule, we obtain

$$p(\hat{D}) / p(\hat{M}^*; \hat{M}_{\star}; \hat{z}; \hat{t}; \hat{A}_V; \hat{z})p(\text{sim})p(D|\hat{D}): \quad (2)$$

This is the fundamental equation that Spoc evaluates. Generically, one would use Equation 2 by beginning with a set of models that uniformly samples the relevant parameter space and then guessing the form of the prior  $p(\hat{M}^*; \hat{M}_{\star}; \hat{z}; \hat{t}; \hat{A}_V; \hat{z})$ , which now encodes the assumed distribution of intrinsic physical properties of galaxies as a function of redshift. In the high-redshift literature, where little is known about the intrinsic physical properties of the galaxies, it is common to neglect priors altogether (or, equivalently, to choose the model with the lowest  $\chi^2$ ) or even to introduce them accidentally by not sampling parameter space uniformly. The difference between this work and that of previous authors is that we account for this prior implicitly by using numerically simulated galaxies as the model set.

To see how this works, consider how one would use Equation 2 in practice. For simplicity, suppose that we wished to constrain a galaxy's stellar mass and that the mass could only fall within one of two ranges. If we omitted priors and assumed that the models sample stellar mass uniformly, then the probability that the galaxy's mass falls within a given range would be given by  $\sum_i A_i e^{-\frac{1}{2}(M^* - M_i)^2}$ , where the sum is taken over all models whose mass lies within that range and the normalization  $A$  is chosen so that the sum taken over all models in both ranges equals unity. If we believed that galaxies with masses in one range were, say, twice as common (and therefore a priori twice as likely to be the right answer) as galaxies with masses in the other

range, we could account for this via an explicit prior by changing the sum to  $\sum_i A_i P_i e^{-\frac{1}{2}(M^* - M_i)^2}$  where  $P_i = 2$  for models in the more common range and 1 for models in the less common range (with  $A$  of course rescaled). It is clear that an equivalent method to employing this explicit prior would be to generate twice as many models in the more common range, resulting in twice the probability of selecting one of these models. Generalizing this idea, one can view simulated galaxies as a Monte Carlo sampling of parameter space that naturally produces more models with parameters that are more commonly found. Hence by taking a set of simulated galaxies, generating a library by resampling this set with parameters having uniform priors (namely,  $A_V$  and  $z$ ), and using that library to discretely sample the probability distribution in the right-hand side of equation 2, one can solve equation 2 effectively incorporating the implicit priors given by the simulated galaxies. This is in essence the Spoc algorithm.

## 2.2 Systematic Uncertainties in Using Simulated Galaxies

One possible problem with this approach is that there is no guarantee that the simulation predicts the correct distribution of intrinsic properties of galaxies; in Bayesian terms, the priors could be wrong. Two of the greatest uncertainties in the input physics for our current simulations are (1) numerical resolution, manifested as an inability to account for physical processes that occur on scales that are too small or too rapid (e.g. merger-induced starburst) and (2) the prescription for superwind feedback. Serious resolution issues will result in poor fits if, for example, the observed ratios of rest-frame UV to rest-frame optical light reflect more bursty SFHs than the models can account for; indeed, this is an example of how Spoc can provide interesting constraints on models. Regarding outflows, we can estimate the extent of any resulting systematics by comparing results from our three different outflow simulations. While this does not span the full range of possible feedback mechanisms, the fact that (as we show in Section 5.1) most of the best-fit parameters are insensitive to the choice of wind prescription suggests that outflows do not noticeably alter typical SFHs at a given stellar mass.

Furthermore, there may be physical processes affecting galaxy SEDs that are not accounted for by our simulation or population synthesis models. In this case, simulated galaxies may have difficulty reproducing the observed spectra, or they may mistakenly model nonstellar contributions to the observed SED as starlight. Among the possibilities here are active galactic nuclei (AGN), incorrectly modeled thermally pulsating asymptotic giant branch (TP-AGB) stars (Maraston et al. 2006), emission lines, and an inappropriate treatment of IGM absorption. We will argue in x6 that significant AGN contamination is unlikely for the high-redshift objects we will consider here. The contribution of TP-AGB stars is also unlikely to be important partly because we do not model measurements from bands redder than  $I$  in the rest-frame, and partly because at  $z > 6$  less than half of the existing stellar mass is more than 200 M yr old (Table 2). Emission lines and incorrectly modeled IGM absorption could in principle affect our results at the 10%

level (Schaerer & Pello 2005; Egami et al. 2005). These effects are expected to be similar for the various SFHs investigated because we use the same population synthesis models to model the stellar continuum in each case. Thus, for the preliminary study in this paper we ignore all these effects.

Another possible problem is that galaxy classes that are rare in reality are likely to be rare in the simulations, so that they will be harder to constrain. For example, our simulations produce no galaxies massive enough at  $z > 6$  to fit the putative  $6 \times 10^1 M_{\odot}$  object at  $z = 6.5$  reported by Mobasher et al. (2005). Although this particular object is likely to be at a lower redshift (Dunlop et al. 2006), it does illustrate limitations imposed by simulation volume, which could also impact constraints on rare classes such as sub-millimeter galaxies (e.g. Smith et al. 2004). In principle one could work around this issue by running larger-volume simulations or by deriving the priors from the simulations and then resampling parameter space by hand. In lieu of these approaches, the simulations utilized must have comoving volumes comparable to the effective volume of the survey in which the object was found.

It may appear overly ambitious to attempt to constrain 6 (or more) seemingly independent parameters for a galaxy for which fewer than 6 measurements are available. However, cosmological simulations allow us to do this because they generically predict that galaxies' intrinsic physical parameters are manifestly not independent; there are tight predicted correlations between, for example, stellar mass on the one hand and star formation rate and metallicity on the other (Finlator et al. 2006; Dave et al. 2006).

In summary, using simulated galaxies to estimate physical properties is only valid when the dominant emission mechanism is star formation, and when other uncertainties can be carefully analyzed and shown to be negligible. For galaxies at high redshift, such as the ones we consider in this paper, this is believed to be true. However, in the general case these issues must be considered carefully. In turn, the goodness of fit enables constraints to be placed on simulations of galaxy formation, and can highlight missing physics that may be required in order to explain the observed properties of galaxies.

### 3 MODELS

#### 3.1 Simulations

We draw our simulated galaxies from cosmological hydrodynamic simulations run with Gadget-2 (Springel & Hernquist 2002), including our improvements as described in Oppenheim & Dave (2006, hereafter OD 06). This code uses an entropy-conservative formulation of smoothed particle hydrodynamics (SPH) along with a tree-particle-mesh algorithm for handling gravity. Heating is included via a spatially uniform photoionizing background (Haardt & Madau 2001), which is an acceptable approximation for the galaxies that are observed at high redshift owing to the fact that they form in highly overdense regions that undergo local reionization at  $z = 6$  (Dave et al. 2006). All gas particles are allowed to cool under the assumption of ionization equilibrium, and metal-enriched particles may additionally cool via metal lines. Cool gas particles are allowed to develop a multiphase interstellar medium via a subresolution

multiphase model that tracks condensation and evaporation following McKee & Ostriker (1977). Stars are formed from cool, dense gas using a recipe that reproduces the Kennicutt (1998) relation; see Springel & Hernquist (2003a) for details. The metallicity of star-forming gas particles grows in proportion to the SFR under the instantaneous recycling approximation. Stars inherit the metallicity of the parent gas particle, and from then on cannot be further enriched.

Cosmological hydrodynamic simulations that do not include kinetic feedback from star formation invariably overproduce stars (e.g., Balogh et al. 2001; Springel & Hernquist 2003a, OD 06). Because superwinds can affect the physical properties of the simulated galaxies (e.g. Dave et al. 2006), we consider model galaxies from simulations with three different superwind schemes: (1) a "no wind" model that omits superwind feedback; (2) a "constant wind" (cw) model in which all the particles entering into superwinds are expelled at 484 km/s out of star-forming regions and a constant mass loading factor (i.e. the ratio of the rate of matter expelled to the SFR) of 2 is assumed (as in the runs of Springel & Hernquist 2003b); and (3) the "momentum-driven wind" (vzw) model of OD 06, in which the imparted velocity is proportional to the local velocity dispersion (computed from the potential) and the mass loading factor is inversely proportional to the velocity dispersion (Murray, Quataert, & Thompson 2005), as inferred from observations of local starbursts (Martin 2005; Rupke et al. 2005). This selection is meant to bracket plausible models in order to expose any related systematic uncertainties; however, owing to the range of successes in comparison with IGM metal-line observations obtained by OD 06 for the vzw model, we focus on this model when the conclusions from the different wind models are broadly similar.

All of our wind models were tested in simulations that assumed the "old" WMAP-concordant cosmology (Spergel et al. 2003) having  $\Omega_m = 0.3$ ,  $\Omega_b = 0.7$ ,  $H_0 = 70 \text{ km s}^{-1} \text{ Mpc}^{-1}$ ,  $\sigma_8 = 0.9$ , and  $\Omega_b = 0.04$ . Each of our simulations has  $2 \times 256^3$  particles, with parameters as given in OD 06. We only employ the  $16h^{-1}\text{Mpc}$  and  $32h^{-1}\text{Mpc}$  simulations from OD 06, as the  $8h^{-1}\text{Mpc}$  runs did not have any galaxies large enough to be observable at  $z > 6$ . An additional set of simulations (the "jzw" model) were run using our preferred wind model with the 3rd-year WMAP cosmology (Spergel et al. 2006), namely  $\Omega_m = 0.26$ ,  $\Omega_b = 0.74$ ,  $H_0 = 71 \text{ km s}^{-1} \text{ Mpc}^{-1}$ ,  $\sigma_8 = 0.75$ , and  $\Omega_b = 0.044$ . In addition to  $16h^{-1}\text{Mpc}$  and  $32h^{-1}\text{Mpc}$  box sizes, we also run a  $64h^{-1}\text{Mpc}$  box to sample the bright end of the mass function in order to better constrain some observed galaxies that we will consider in x6. There is a slight difference in jzw versus vzw, in that jzw has a smaller mass loading factor by a factor of two-thirds compared to vzw (in the terminology of OD 06,  $\Omega_b = 200 \text{ km/s}$ ) in order to compensate for the lower collapse fraction at high redshift in the new cosmology. We found that model galaxies from the jzw simulations have bulk properties that are similar to that from vzw. Sproc computes all luminosity distances assuming the new 3rd-year WMAP cosmology.

We identify galaxies using Spline Kernel Interpolative DENMIX (see Kerec et al. 2005 for a full description). We only consider galaxies with stellar masses exceeding 64 star

particles, which represents a converged sample in terms of both stellar mass and star formation history (Finlator et al. 2006). According to this criterion, our  $16h^{-1}Mpc$  simulation volumes resolve galaxies with stellar mass  $\gtrsim 1.2 \times 10^9 M_{\odot}$ .

For this work, the most important output of the simulations is the set of SFHs corresponding to the resolved galaxies in each simulation at the various redshift outputs. We obtain the rest-frame spectrum for each star formation event in a given galaxy at the time of observation by interpolating to the correct metallicity and age within the Bruzual & Charlot (2003) models, assuming a Chabrier IMF. Summing these up, we obtain the galaxy's intrinsic rest-frame spectral energy distribution (SED).

We consider the following prescriptions for dust reddening: The Calzetti et al. (2000) starburst dust screen, the Charlot & Fall (2000) embedded star formation law, the Gordon et al. (2003) Small Magellanic Cloud bar law, and the Cardelli et al. (1989) Milky Way law. We account for IGM absorption bluewards of rest-frame Ly using the Madau (1995) prescription. The Madau (1995) law may be less appropriate for  $z \gtrsim 6$  than at lower redshifts because the universe is completing reionization at this epoch. Indeed, Schaefer & Pello (2005) found that they were able to improve the quality of their fits to the SEDs of two reionization-epoch galaxies by simply doubling the optical depth predicted by Madau (1995). However, they also found that the best-fit derived parameters are relatively insensitive to the IGM treatment. Thus, for simplicity we retain the Madau (1995) treatment without modification.

### 3.2 One-Parameter Star Formation Histories

To date, efforts to use SED-fitting to infer the physical properties of high-redshift galaxies have generally employed some combination of constant, exponentially decaying, and single-burst star formation histories in order to span the presumed range of possibilities. In general, it has been found that the stellar mass, SFR, and redshift of a galaxy can be fairly well-constrained via this technique while the age, metallicity, and dust extinction cannot. Much of the gain in precision that results from using simulated galaxies in SED-fitting results from the relatively small range of SFHs that actually occur in the simulations.

For example, the solid black curves in Figure 1 show the SFHs of the 3 galaxies from the vzw simulation that yield the best fits to the  $z = 6.7$  galaxy Abell 2218 KESR, which we will discuss extensively in §5. The SFHs have been sampled in 20-Myr bins and smoothed with a 100-Myr tophat in order to make the plot more readable. All 3 galaxies begin forming stars at  $z > 15$  and exhibit a SFR that is generally rising. An examination of simulated SFHs at these redshifts shows that steadily rising SFHs are typical. For this reason we consider a constantly-rising toy model SFH in this work; as we will see, the constantly-rising model reproduces most closely the constraints obtained from the simulated galaxies (Figure 6). This model has to our knowledge not been investigated before.

In order to facilitate comparison with much of the available SED-fitting work that is available in the literature, we investigate three toy model SFHs for each galaxy in addition to simulated SFHs, as described below:

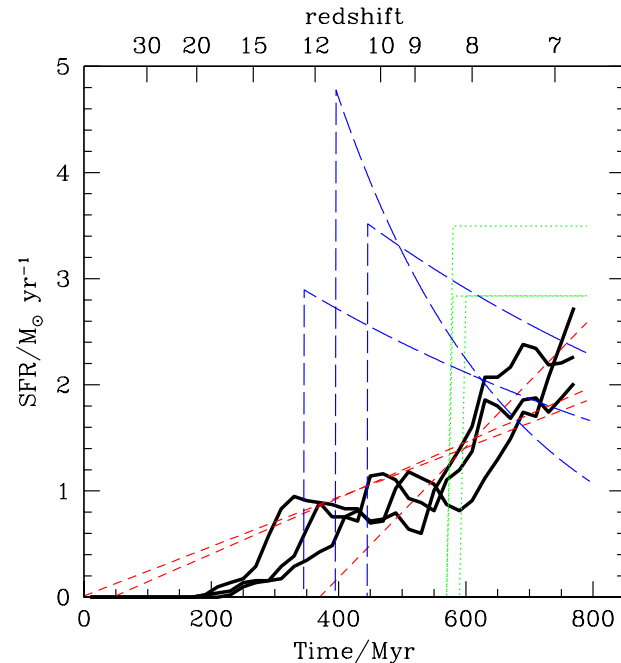


Figure 1. Star formation histories of the 3 best-fitting vzw galaxies for Abell 2218 KESR, along with the 3 best-fitting galaxies from each of our toy model SFHs. The SEDs of all models match the data with  $\chi^2$  per degree of freedom less than unity. The vzw SFHs have been sampled in 20-Myr bins and smoothed with a 100-Myr tophat for readability. The areas under the curves are slightly different, reflecting uncertainty in the total stellar mass. Note that the best-fitting rising model is very similar to the best-fitting simulated model.

Exponentially Decaying SFR We generate models with SFR proportional to  $e^{-t/t_{\text{dec}}}$ . We use four values of  $t_{\text{dec}}$  logarithmically spaced between 10 and 795 Myr, roughly the age of the universe for our most distant object. Each of these SFHs is sampled at 23 ages evenly spaced between 10 and 1000 Myr.

Constant SFR We generate models that have been forming stars at a constant rate  $M_{\odot} \text{ for } t \text{ Myr}$ . For we sample 41 ages that lie between 10 and 1000 Myr, and for  $M_{\odot}$  we sample 45 SFRs that lie between 0.2 and 30.0  $M_{\odot} \text{ yr}^{-1}$ .

Constantly Rising SFR In the constantly rising SFH, a galaxy's SFR is proportional to the amount of time that has passed since it formed its first stars. While a rising SFH can clearly not be maintained for all galaxies until low redshifts, it arises fairly generically for high-redshift galaxies in hydrodynamic simulations (Finlator et al. 2006). We generate models in which each galaxy's SFR has been rising at a constant rate  $M_{\odot} \text{ for } t \text{ Myr}$ , where for  $t$  we have sampled 41 ages that lie between 10 and 1000 Myr.

For each star formation history, we have generated models with masses in the range  $\log(M_{\odot}) \in [7.5; 10.5]$  and metallicities  $Z = Z_{\odot} (0.005; 0.07; 1.0; 2.5)$ . These SFHs are then put through the Spoc formalism, in order to determine the probability distribution of physical properties. During the fitting, we require that the oldest star of a given model is not older than the age of the universe at the model's redshift.

## 4 P E R F O R M A N C E O F Spoc

## 4.1 SelfC onsistency Test

We begin by testing that Spoc recovers the (known) properties of simulated galaxies. This serves to both test and quantify the intrinsic uncertainties of the algorithm. To do so, we take the 73 galaxies that are resolved by our vzw simulation at  $z = 6.5$ , and determine how accurately we can recover their intrinsic physical properties using model galaxies from the  $z = 6$  and  $z = 7$  outputs as inputs to Spoc. While the model and sample galaxies are not strictly independent in this test (all but the least massive galaxies at  $z = 6.5$  correspond to at least one ancestor in the  $z = 7$  output and descendant in the  $z = 6$  output), the galaxies are evolving rapidly enough that these populations are effectively independent. The test-case and model galaxies are compared in 6 bands from i-band to IRAC 4.5 m (the same ones applied to Abell 2218 KESR in x5), where we assume a 0.15 magnitude uncertainty in each band. The test-case galaxies are reddened with a fiducial dust extinction  $A_V = 0.6$  via the Calzetti et al. (2000) law; however, we find essentially identical results for different values of the dust extinction. During the fitting, redshift space is sampled by perturbing each model galaxy over a grid extending to  $z = 0.5$  and  $A_V$  is sampled over the range  $A_V \in [0, 1]$ .

Spoc constrains six quantities:  $M$ , SFR,  $A_V$ ,  $Z$ , age, and redshift. The definitions of  $M$  and redshift are self-evident.  $A_V$  is defined in terms of the Calzetti et al. (2000) reddening prescription. For the purposes of this work, metallicity  $Z$  is defined as the mean mass fraction of metals in the galaxy's stars; this is useful in determining what metallicity to choose during population synthesis modeling. Although metallicity is not the dominant factor in determining a galaxy's SED, the fact that the vzw model reproduces the mass-metallicity relation of star-forming galaxies at  $z = 2$  (Frb et al. 2006) as well as for the host galaxy of GRB 050904, which is located at  $z = 6.295$  (Berger et al. 2006; Kawai et al. 2006), leads us to believe that this model's predictions for the metallicities of observed reionization-epoch galaxies are plausible (Finlator et al. 2006, in prep.). We define a galaxy's age as the mass-weighted mean age of its star particles; this is more meaningful than the more commonly-used age of the oldest star, which is both difficult to constrain observationally and difficult to predict owing to the stochastic nature of our simulations' star formation prescription. We define a galaxy's SFR as the average over the last 100 M yr leading up to the epoch of observation; if none of a galaxy's stellar mass is older than 100 M yr then the age of the oldest star is used. This metric is found to correlate more tightly with rest-frame UV flux than averages over a shorter time-baseline for the numerically simulated SFHs.

Figure 2 shows how the fractional error in the six inferred properties varies with stellar mass. The dotted lines indicate the mean formal 1 uncertainties; these are computed directly from the probability densities that are returned by Spoc rather than from the scatter in Figure 2. In general, the recovered physical parameters lie within 50% and 2 of the correct values, suggesting that our SED-fitting technique is indeed self-consistent. The fact that the formal uncertainties are at least as large as the scatter (and, in

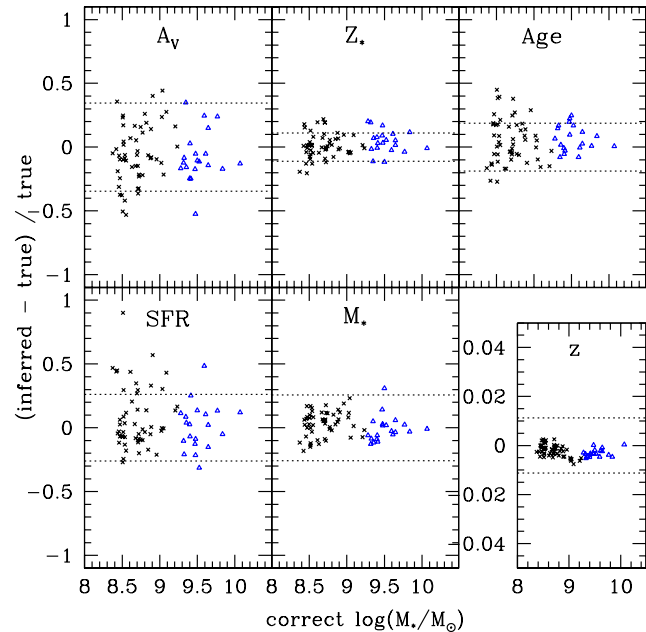


Figure 2. Fractional error in inferred physical properties of  $z = 6.5$  vzw galaxies as determined using the  $z = 6.0$  and  $z = 7.0$  galaxies as models in Spoc. Black crosses and blue triangles denote model galaxies from the  $16h^{-1} Mpc$  and  $32h^{-1} Mpc$  volume simulations, respectively. Dotted lines indicate mean fractional uncertainties computed by Spoc. With few exceptions, the best-fit values are within 50% and 2 of the correct values. Stellar mass and redshift are recovered remarkably accurately.

some cases, are somewhat larger) suggests that the formal uncertainties are sufficiently conservative.

The most accurately (and precisely) recovered parameter is redshift. The high accuracy in this case owes to the fact that the  $I_{814}$ ,  $z_{850}$ , and  $J_{110}$  fluxes tightly constrain the position of the Lyman break, which itself results from the Madau (1995) prescription for IGM absorption.

Stellar mass is recovered with 20% accuracy, owing primarily to the fact that the rest-frame optical flux is generally dominated by numerous long-lived, low-mass stars whose mass-to-light ratio is relatively insensitive to age and dust extinction. Additionally, as we will show in Figure 3, the lack of a significant systematic offset in the recovered stellar masses owes to the similarity between the SFHs of the test-case and model galaxies.

Metallicity is also accurately recovered. This is expected given that there is a tight mass-metallicity relation in the simulations (the 1 scatter is 15%) that does not vary strongly with redshift (Davé et al. 2006), and the fact that the test galaxies and models come from the same simulations. Without this implicit prior, metallicity cannot be tightly constrained from broadband photometry (Papovich et al. 2001; Schaefer & Pello 2005).

Turning to SFR, we expect a reasonably accurately inferred SFR given the tight correlation between SFR and stellar mass that the simulated galaxies obey (Finlator et al. 2006; Davé et al. 2006); in other words, if the redshift is known and the stellar mass can be constrained from the rest-frame optical flux, then the SFR is already constrained

to within a factor of two regardless of the rest-frame UV flux. Figure 2 bears this out. In detail, SFR is somewhat less accurately recovered than stellar mass owing to the degeneracies with age and  $A_V$ ; in fact, a close inspection reveals that galaxies with underestimated SFR have overestimated  $A_V$  and vice-versa.

Age is accurately recovered owing largely to the small range of SFHs that occur in our simulations. Just as only a small range of metallicities remains available once the stellar mass is constrained, a relatively small range of ages is available once the redshift and stellar mass are constrained (Figure 1).

In this way, stellar mass, metallicity, age, and SFR can simultaneously be recovered by Spoc when numerically simulated models are used owing to the existence of implicit priors on these parameters. Any remaining discrepancy between the observed and model UV fluxes is minimized by the choice of  $A_V$ , which is also relatively accurately recovered.

In a separate experiment, we generated test-cases with one dust extinction curve and attempted to recover their properties under the assumption of a different curve. We found that all of the physical parameters were accurately recovered (including  $A_V$ , although this is not expected generically) except redshift, which was systematically off at the 1–2% level depending on  $A_V$ . This therefore constitutes a minimum uncertainty to the photometric redshifts that are obtained via SED fitting.

#### 4.2 Comparison With Toy Models

It is reassuring but not terribly surprising that Spoc can accurately recover the physical properties of the galaxies that it uses as templates. A more interesting question is how well Spoc can recover galaxy properties using a different SFH than that of the input galaxy, as this illustrates the variations in inferred physical parameters among various assumed SFHs. To address this, we have fit the test-case galaxies that were used in Section 4.1 using model sets generated from constant, decaying, and rising SFHs as described in Section 3.2.

Figure 3 gives the distributions of fractional errors in the inferred values of stellar mass, SFR, age, and redshift that result when using the different model sets. The vzw case is simply a vertically-binned histogram from Figure 2. Generally, the toy models yield stellar mass and age results that are within 50% of the correct values. The errors for these quantities are generally distributed with slightly larger scatter than the errors from the vzw models and show systematic discrepancies up to the 40% level. The SFRs are overestimated systematically by 50–200% with significantly more scatter than returned by the vzw models; this is clearly the quantity that is most dependent on the assumed SFH. The vzw models systematically underestimate redshift by 0.2% while the toy models are low by 0.5%; the scatters are comparable for all of the models. We briefly discuss results specific to each toy model in turn.

When considering all test-case galaxies together, the constant-SFR models tend to underestimate the age and stellar mass by 40% and 10% respectively while overestimating the SFR by a median factor of 3, the largest discrepancy among the SFHs that we consider. When we split the sample into “massive” and “low-mass” galaxies at  $M = 10^9$ ,

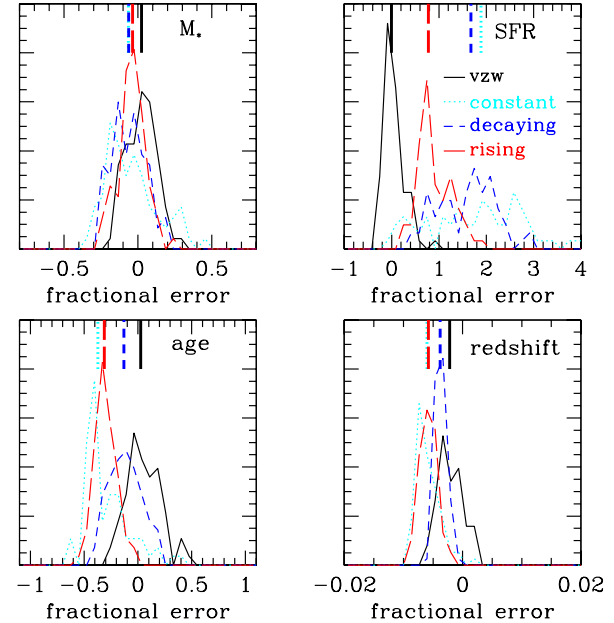


Figure 3. Comparison of the distribution of fractional errors in the inferred physical properties of the galaxies from Figure 2 when assuming different SFHs in Spoc. Redshift error is plotted as  $z = (1 + z)$ . All histograms in a given plot have been normalized to enclose a constant area. Solid black, dotted cyan, short-dashed blue, and long-dashed red curves give the histograms for the simulated, constant, decaying, and rising model sets; the vertical tick-marks at the top indicate the respective medians. Redshift is very well-recovered for all models, stellar mass and age to within 50%, while SFR can be off by large amounts.

we find that the constant models tend to overestimate the ages of “massive” galaxies by ~20% while underestimating the ages of low-mass galaxies by ~40%. In order to match the rest-frame optical measurements, the constant-SFR models then overestimate the SFR for the low-mass and massive galaxies by 100–200% and 0–100%, respectively, with 50% scatter in each case. Stellar masses are underestimated by 20% for the low-mass galaxies and overestimated by roughly the same amount for massive galaxies. This illustrates that uncertainties in parameter recovery are not only dependent on the assumed SFH, but also on the mass.

The decaying models tend to reproduce the stellar mass and age with systematic errors of roughly 10% and scatter comparable to the scatter from the vzw models. These successes are somewhat surprising because the simulated SFHs look nothing like the decaying case. Conversely, the SFRs are higher by a median factor of 2.8, only slightly better than the constant model. The fact that the SFR could be dramatically overestimated while the age, stellar mass, and dust reddening (not shown) are recovered accurately probably owes to our use of 100-M yr average SFRs. When considering all of the stellar mass that has formed in the last 100 M yr, a larger fraction of the O-stars will have evolved off of the main sequence for decaying or constant SFHs than for rising models that show the same 100 M yr average SFR, leading to the result that models with decaying SFRs nonetheless produce similar UV luminosities. The broad success of the

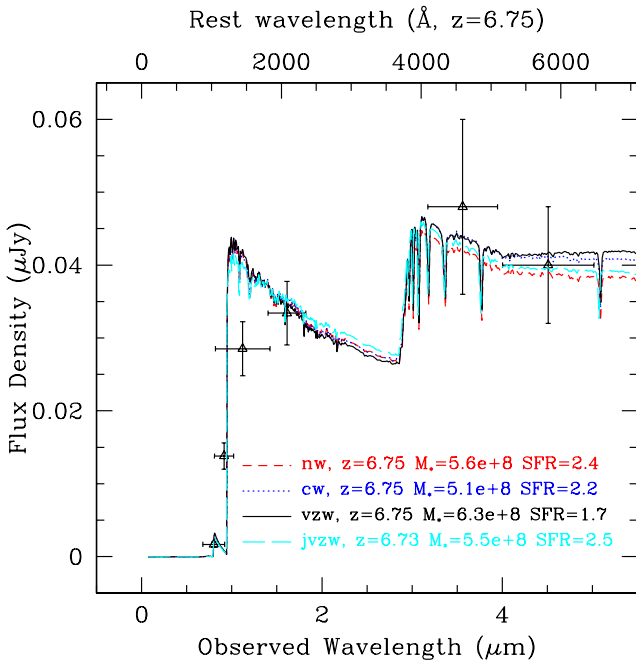


Figure 4. Best-fit spectra from the simulations to the data for Abell 2218 KESR, which we have demagnified by 25 (Kneib et al. 2004). Spectra from the nw, cw, and vzw, and jvzw models are denoted by red dashed, blue dotted, black solid, and long-dashed cyan curves, respectively. All four models produce galaxies whose spectra match Abell 2218 KESR within the errors ( $\chi^2$  per degree of freedom  $< 1$ ).

decaying model despite the input SFHs looking nothing like the decaying case shows that SED fitting can yield interpretations consistent with monolithic collapse models even though the true SFH may be quite different.

The rising models tend to underestimate the age by 10–40% and overestimate the SFR by 40%, though with significant scatter. Both of these sets are compensated by overestimated  $A_V$  in such a way that the stellar masses are recovered quite accurately, with  $< 5\%$  systematic offset and scatter comparable to what is achieved via the numerically-simulated models. Overall, this model probably recovers the true parameters most faithfully among the toy models, though it is not a dramatic improvement over the others.

In summary, we have shown that Spoc can self-consistently recover the physical properties of the model galaxies that we use in fitting observed high-redshift galaxies. Further, toy models are able to recover stellar mass and age to within 50% accuracy and SFR to within a factor of three, although there are systematic offsets at a comparable level. All models yield photometric redshifts with better than 1% accuracy although none of them outperform the numerical models.

## 5 TEST CASE: ABELL 2218 KESR

The triple arc in Abell 2218, dubbed Abell 2218 KESR by Schaefer & Pello (2005) after its discoverers (Kneib et al.

2004), is probably the best-studied  $z > 6$  object, and its physical parameters have been constrained through SED fitting by various authors. Hence it provides a good test case for exploring the systematics that result from using numerically simulated model galaxies, and comparing to results employing more traditional simple SFHs.

The flux from Abell 2218 KESR can be measured from two lensed images in the Hubble Advanced Camera for Surveys (ACS)  $z_{850}$ , Wide-Field Planetary Camera 2 (WFC2)  $I_{814}$ , and Near-Infrared Camera and Multi-Object Spectrograph (NICMOS)  $J_{110}$  and  $H_{160}$  bands, and only one image in the Spitzer/IRAC 3.6 and 4.5  $\mu\text{m}$  bands (the other image is blended with a nearby submillimeter source at IRAC's spatial resolution). Schaefer & Pello (2005) note that the fluxes measured by different authors in the optical/near-infrared bands disagree due to the inherent difficulties of measuring photometry from extended arcs, and that the different images of the galaxy do not agree in the Hubble/ACS  $z_{850}$  band. Following their suggestion, we use the weighted mean of the two images in the optical/near-infrared bands (their SED 1) and impose a minimum 0.15  $\mu\text{m}$  uncertainty in all bands in order to account for differential lensing across the images.<sup>2</sup>

### 5.1 Wind Model and Dust Prescription

Figure 4 shows that the SEDs of the best-fitting model galaxies from our three feedback recipes and two cosmologies all reproduce the observations with reduced  $\chi^2 < 1$ . Moreover, they are remarkably similar. All four models possess a very blue rest-frame UV continuum owing to young age and low metallicity as well as a pronounced Balmer break owing to the presence of older stars. The best-fit parameters are similar, indicating that the simulation's ability to reproduce the observations is robust to the choice of superwind feedback prescription and cosmology (to the extent of the variations considered). This result is akin to the findings from studies employing toy model SFHs that good fits can be obtained via a variety of assumed SFHs and metallicities.

To quantify this point, Figure 5 and Table 1 show how the derived probability densities for the physical parameters of Abell 2218 KESR depend on the choice of wind model. The entries in Table 1 list the mean and variance of the histograms shown in Figure 5. Each curve in Figure 5 has been normalized to unit area and then scaled so that all four curves fit on the same plot.

All of the derived physical parameters except  $Z$  are remarkably robust to our choice of superwind feedback prescription. Generally, the data seem consistent with negligible dust reddening, a mean stellar age of 100–200  $\text{Myr}$ , SFRs of 1–3  $\text{M}_\odot \text{yr}^{-1}$ , a stellar mass of  $3.8 \times 10^9 \text{M}_\odot$ , and a redshift  $z = 6.7$ , in good agreement with other determinations (Egami et al. 2005; Schaefer & Pello 2005)<sup>3</sup>. The

<sup>2</sup> Schaefer & Pello (2005) have noted that the published upper limits from LRS and in the Hubble/ACS  $V_{606}$  band do not significantly affect the derived parameters. In the case of the  $V_{606}$  limit, we have verified this.

<sup>3</sup> Note that because our simulations' star formation treatment assumes instantaneous recycling, we give here the total mass of stars that have formed. Using the Bruzual & Charlot (2003) tables, we find that 70% of the stellar mass of stars formed in

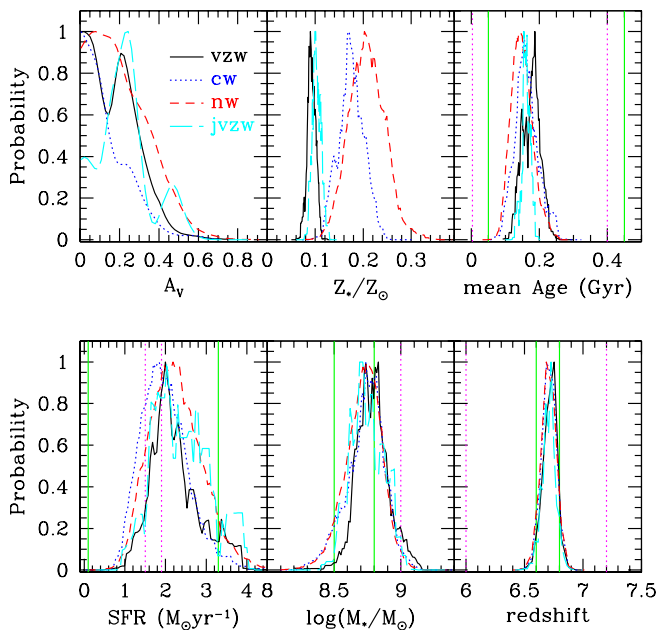


Figure 5. Probability densities for the physical parameters of Abell 2218 KESR based on four numerical simulations assuming different treatments for superwind feedback. Results from the nw, cw, vzw, and jvzw models are given with dashed red, dotted blue, solid black, and long-dashed cyan lines, respectively. Solid green and dotted magenta boundaries denote ranges inferred by Egami et al. (2005) and Schaefer & Pello (2005), respectively (the lower limit to stellar mass obtained by Schaefer & Pello (2005) is 7.7). Each curve has been normalized to unit area and then scaled so that the three models fit on the same plot. All of the best-fit physical parameters except metallicity (see text) are robust to changes in the superwind feedback treatment.

tightness of the constraints on the various intrinsic physical parameters results from the relatively narrow range of SFHs experienced by the galaxies in the simulations. By contrast, the uncertainty in the inferred redshift is determined by our treatment of IGM extinction since the inferred redshift is dominated by the position of the Lyman- $\alpha$  break.

Comparing the results from the models in detail, both the cw and nw models are less efficient at suppressing star formation via wind feedback. For this reason, at fixed number density (or equivalently, dark matter halo mass) the cw and nw model galaxies have formed more stars, retained more of their metals, have a higher SFR, and are older (Davé et al. 2006). Similarly, at a given stellar mass, the vzw galaxies are younger, have expelled a larger fraction of their heavy elements, and for these reasons require more dust reddening in order to match a given observed colour owing to the age-metallicity{dust degeneracy. The jvzw models give results that are similar to the vzw results owing to the similar feedback treatment. However, the lower values used in the jvzw simulation for the cosmological parameters  $m$  and  $\sigma_8$  delay the growth of structure at early times, yielding fewer model galaxies for us to match against observations for a given simulated volume. As a result, parameter

galaxies that are more massive than  $10^8 M_{\odot}$  at  $z = 6.75$  remain in stellar form at  $z = 6.75$ .

space is less well-sampled and the probability density curves (notably  $A_v$ ) exhibit more structure.

Next to stellar mass and redshift, the mean stellar metallicity is the most tightly constrained parameter, followed by the mean age and SFR. Metallicity is the only parameter for which the different wind models disagree at the  $> 1\sigma$  level. That the models could agree on all of the derived parameters except for the metallicity reflects the fact that the effect of metallicity on the photometry is small compared to the effect of stellar age (Schaefer & Pello 2005). On the other hand, the tightness of the metallicity constraint follows from the tight mass-metallicity relation that the simulation predicts (Section 4). Thus, the apparent disagreement between the metallicity constraints is simply a reflection of the tight priors imposed by the different simulations combined with the robust constraints on stellar mass. Note that because the vzw model agrees the best with the distribution of metals in the IGM (OD 06) and the mass-metallicity relationship of star-forming galaxies (Finkbeiner et al. 2006, in preparation), it probably makes the most believable prediction of Abell 2218 KESR's mean stellar metallicity.

We investigated the effect that varying the dust prescription has on the derived physical parameters and found, in agreement with Schaefer & Pello (2005), that this has no significant effect on the derived physical parameters other than  $A_v$ . The derived  $A_v$  were roughly 0.1 mag lower for the Cardelli et al. (1989) and Charlot & Fall (2000) laws; these differences are expected given the extra extinction imposed at rest-frame UV wavelengths in the former case and (similarly) for younger stars in the latter case. The total amount of light removed by dust extinction, which can be regarded as a prediction of the total infrared luminosity, is roughly  $10^{10} L_{\odot}$ , independent of the assumed dust prescription.

Two groups have previously published constraints on this object's properties. Egami et al. (2005) employed a uniform sampling of single-parameter SFHs; their results are given in Table 1 and by the solid green vertical lines in Figure 5, where we have converted their derived SFR and  $M_{\star}$  to values appropriate for a Chabrier IMF. It is clear that their constraints are entirely consistent with our own, although the tight intrinsic correlations between physical parameters in the simulated models allow us to impose tighter constraints on all of the derived parameters. In the second work, Schaefer & Pello (2005) exhaustively examined the systematics of assumptions regarding SFH and template spectra with the goal of bracketing the most likely parameter space. Their constraints are given by the dotted magenta vertical lines and are also listed in 1; these constraints are also consistent with ours. Thus, to the extent that our simulated galaxy spectra are representative of the spectra of high-redshift galaxies, our models offer a physically-motivated way to obtain the tightest possible constraints on the underlying properties of these objects.

## 5.2 Comparison to Toy Model SFHs

Efforts to constrain the physical properties of high-redshift galaxies via SED-fitting invariably encounter a host of degeneracies between the best-fit parameters, the most difficult of which is certainly the age-extinction-SFR degeneracy (Shapley et al. 2001; Papovich et al. 2001;

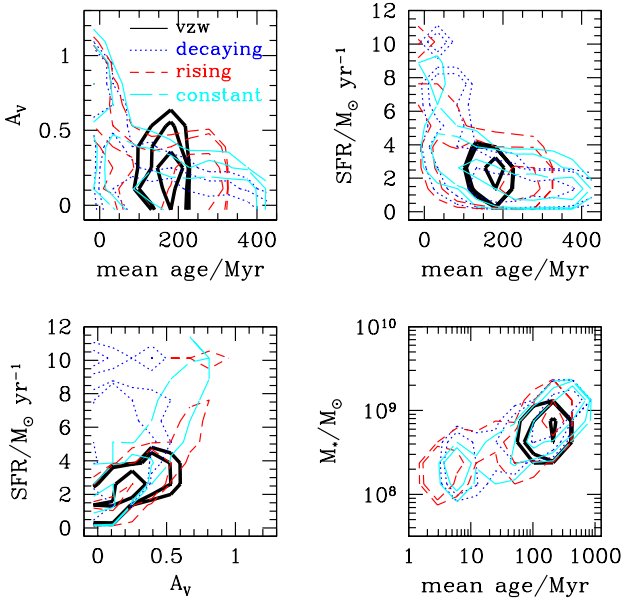


Figure 6. Best-fit combinations of age, extinction, and SFR for 1000 Monte Carlo re-observations of Abell 2218 KESR. The solid black, dotted blue, short-dashed red, and long-dashed cyan contours enclose 68%, 95%, and 99% of the best-fit solutions for the vzw, decaying, rising, and constant model sets, respectively. The vzw models allow for the tightest constraints to be placed. Interestingly, the 1 best-fit intervals from the constantly-rising SFH are very close to the simulation result.

Shapley et al. 2005). Generally, young stellar population age, high SFR, and low dust extinction all yield bluer photometric colours while old age, low SFR, and high dust extinction all yield redder photometric colours. These degeneracies also contribute to the uncertainty in the inferred stellar mass via the stellar age-stellar mass degeneracy, whereby older populations have a higher mass-to-light ratio, yielding a higher stellar mass at a given measured flux density. Compounding the problem, there are a number of ways in which the best-fit physical properties depend on any assumptions that are made regarding the shape of a galaxy's star formation history (Shapley et al. 2005). The simplicity of working with numerically simulated galaxies is that the only assumption one is required to make is that the numerical simulations reproduce the range of SFHs that actually occurs in nature (though this is admittedly a significant assumption). Adopting this assumption excludes a wide range of parameter space, tightening constraints on parameters that depend strongly on the shapes of the trial SFHs.

In order to show how effective the simulations are at reducing well-known degeneracies in best-fit parameters, we generated 1000 Monte Carlo re-observations of Abell 2218 KESR by adding scatter to the photometric measurements in a way that was consistent with the reported observational uncertainties. For each data set, we then determined the best-fit parameters from the vzw models as well as from the decaying, rising, and constant SFH models. Figure 6 shows the locus of best-fit parameters in several famously degenerate projections of parameter space. The solid black, dotted

blue, short-dashed red, and long-dashed cyan contours enclose 68%, 95%, and 99% of the best-fit solutions for the vzw, decaying, rising, and constant model sets, respectively.

The expected degeneracies that result from toy model SFHs are easy to see in each panel of Figure 6. At the young end, each of the toy models includes a parameter space corresponding to a galaxy that has formed all of its stars in a rapid burst lasting less than 100 Myr. Our use of 100-Myr average SFRs guarantees these models a high SFR ( $> 4 M_{\odot} \text{ yr}^{-1}$ ). Because these models are very young, they are intrinsically blue and can require high dust reddening ( $A_v \gtrsim 1 \text{ mag}$ ) to match the observations. Additionally, their young ages guarantee that their observed optical flux is dominated by short-lived O and B stars with low mass-to-light ratios, leading to low inferred stellar masses. These dramatic burst-dominated models have no analogue in the simulations.

The old end is dominated by the constant-SFR models, equivalent to the  $\tau = 1$  limit of the decaying models. These models are characterized by intrinsically red colours and high mass-to-light ratios, leading to low dust extinctions and high stellar masses. The oldest of these fits requires the galaxy to have been forming stars at  $1 M_{\odot} \text{ yr}^{-1}$  when the universe was less than 10 Myr old; our simulations cannot produce this because gas densities have not grown high enough to support such SFRs at such early times.

At the 1 confidence level, the toy model that most closely approximates the simulated galaxies is the rising SFH model, albeit with a preference for somewhat older ages. Returning to Figure 1, we see that this is expected because the simulated galaxies' SFHs are generically characterized by a slowly rising SFR at these redshifts. Conversely, at the  $\approx 2$  level, the constantly rising SFH model allows for a wider range of models that have no analogues in the simulations. The relatively small range of simulated galaxy SFHs typical by the examples in Figure 1 leads directly to the relatively tight range of inferred ages for the solid contours in Figure 6. Assuming that Abell 2218 KESR is located at  $z = 6.75$ , the SFHs in Figure 1 suggest that it may have formed its first stars before  $z = 15$ , with (10%, 50%) of its stars in place by  $z = (11, 8)$ ; in other words, roughly half of the best-fitting models' stars at the epoch of observation are over 150 Myr old. This relatively old population readily accounts for the pronounced Balmer break that is visible in Figure 4, and is typical in our simulations.

In summary, the chief point of this paper is clearly demonstrated by the fact that, in each panel of Figure 6, the confidence intervals obtained from simulated galaxies fall well within the range described by the complete set of toy model SFHs, while clearly yielding the tightest constraints. The tighter constraints owe to the relatively small range of SFHs and the tight correlations between the various parameters that generically occur in hierarchical simulations of galaxy formation. Given the broad success of the vzw model in matching a variety of data, we suggest that these constraints can be taken reasonably seriously. Of course, the true test will come when spectra are obtained for galaxies such as Abell 2218 KESR, whereby the physical parameters can be more directly inferred from observations and compared to those derived from Spoc.

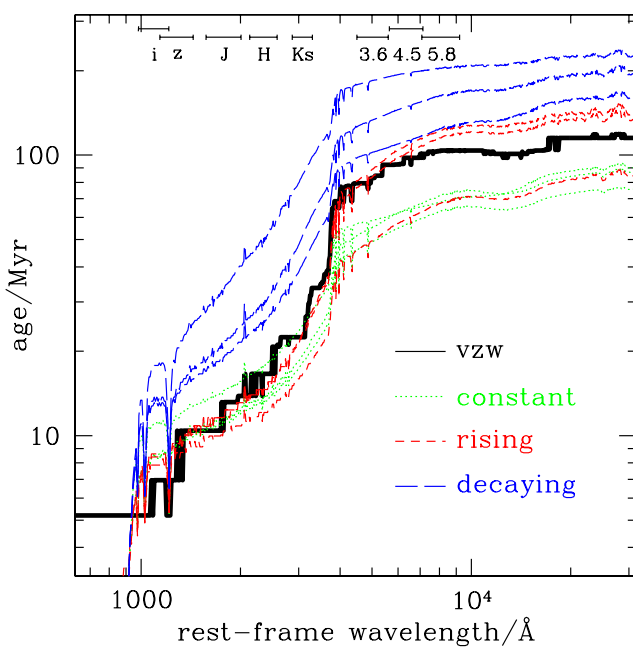


Figure 7. Light-weighted median age of A 2218 KESR versus rest-frame wavelength. The single solid curve corresponds to the best-fitting vzw model while the dotted green, short-dashed red, and long-dashed blue curves correspond to the three best-fitting constant, rising, and decaying models, respectively. The ranges at the top of the figure indicate the full width at 20% of maximum response for an object located at  $z = 6$ . The specific toy models whose spectra are considered in Figure 7 are the same as the models in Figure 1 except that we include only the best-fitting vzw model for clarity. Generally, measurements shortward of the Balmer break sample light from stars that are 50–100 Myr old whereas measurements in rest-frame optical wavelengths constrain older populations.

### 5.3 The Importance of Rest-Frame Optical Data

In this work we focus on reionization-epoch objects for which rest-frame optical measurements are available because the rest-frame optical flux is dominated by relatively low-mass stars whose mass-to-light ratio evolves slowly relative to the stars that dominate the rest-frame UV. For reasonable SFHs, this allows tighter constraints to be placed not only on the galaxy's stellar mass, but also on its SFH. To quantify this point, Figure 7 plots the light-weighted median age of A 2218 KESR versus rest-frame wavelength for the SFHs in Figure 1. For example, a point at 2000 Å and 15 Myr indicates that, for that model, 50% of the photons with rest-frame wavelength of 2000 Å are emitted by stars that are 15 Myr old or younger.

For all of the models that we consider, photons from bluewards of the Balmer break are generated by stars that are under 100 Myr old. This is expected since B stars live roughly 100 Myr (Iben 1967) and justifies the use of rest-frame UV flux as a constraint on the current SFR. Conversely, it explains why rest-frame UV data do not constrain a galaxy's SFH prior to 100 Myr before the epoch of observation. By contrast, data from longer wavelengths sample the SFH at earlier epochs because the stars that dominate these wavelengths live much longer. In the case of A 2218

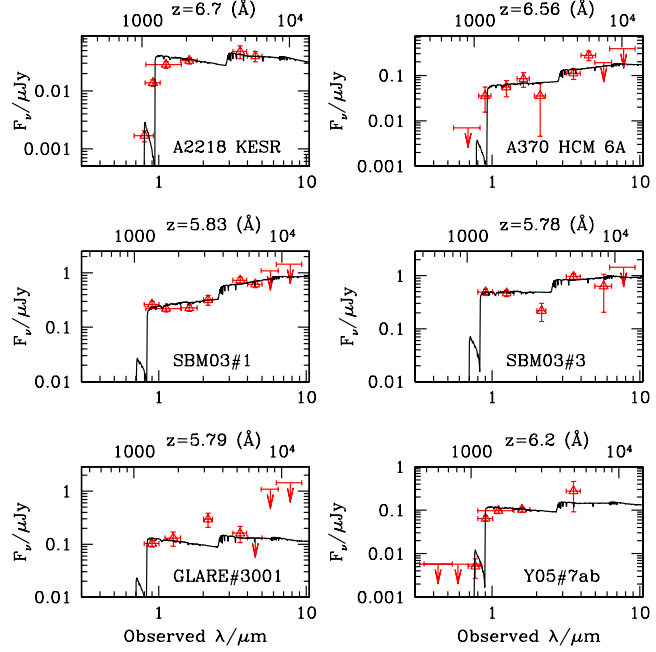


Figure 8. Spectra of the best-fitting model galaxies overplotted on the measured photometry. In cases where spectroscopic redshifts are available this has been forced; in other cases (Abell 2218 KESR and Y05#7ab) we used the photometric redshifts. Horizontal error bars indicate the full width of each filter at 20% of maximum response. The bottom and top horizontal axes give the observed and rest-frame wavelengths. Using the numerically-simulated SFHs with the Bruzual & Charlot (2003) models, we obtain satisfactory fits in all cases and excellent fits in 5 cases.

KESR, the constant and decaying models in Figure 7 suggest that rest-frame optical data constrain the galaxy's SFH roughly 80 and 200 Myr before the epoch of observation, while the rising and vzw models fall in between these limits; the differences probably owe to the detailed interplay between the slope of the SFH and the rate at which low-mass stars fade. It is possible that the rough agreement in the optical portion of Figure 7 explains the tendency of all of the best-fitting models in Figure 1 to be in rough agreement with each other during the interval  $z = 8$ –6.7 even though they diverge prior to  $z = 8$ . Note that this agreement is nontrivial given that all of the toy models can in principle match the observations with burst-like solutions (Figure 6). Most importantly, it highlights the potential of rest-frame optical measurements redwards of the Balmer break to constrain the SFH for reionization-epoch galaxies.

### 6 A SAMPLE OF REIONIZATION-EPOCH GALAXIES

While the example of Abell 2218 KESR is illustrative, the ultimate purpose of Spoc is to constrain physical parameters for a large sample of galaxies, in order to characterize the observed galaxy population and to constrain the underlying galaxy formation model. To illustrate the sort of insights gained using Spoc, we apply it to a sample of observed  $z > 5.5$  objects that have published broadband photometry in the rest-frame UV and optical bands. For each object,

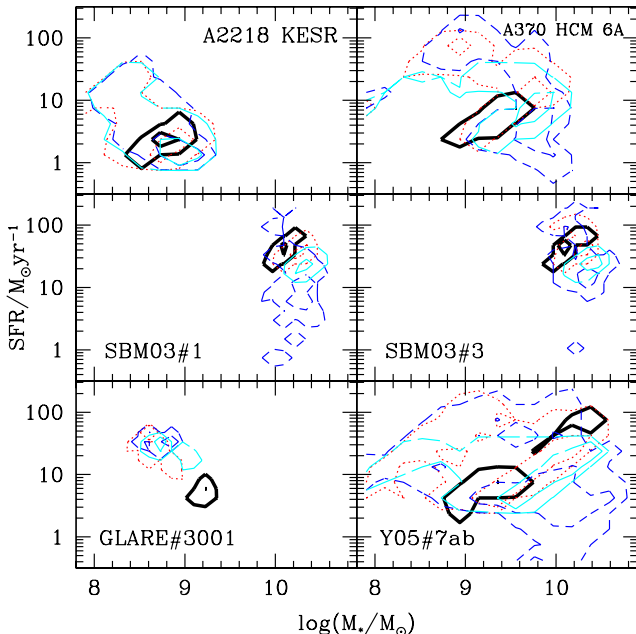


Figure 9. Contours enclosing 68 and 99% of the solutions found for the various galaxies given the various SFHs that we inspected. Thick solid black, dotted red, solid cyan, and dashed blue curves correspond to the  $j_{\text{yzw}}$ , rising, constant, and decaying SFH models, respectively. In all cases but GLARE # 3001, the  $j_{\text{yzw}}$  models yield results that are generally consistent with the toy model SFHs while allowing for equally-tight or tighter uncertainties.

we used Spoc to determine its best-fit physical parameters with the  $j_{\text{yzw}}$ , constant, rising, and exponentially-decaying models. For objects whose redshift has been measured spectroscopically, we run Spoc twice: once with the redshift constrained to the measured value and once with the redshift left as a free parameter. The first run allows more accurate derivations of the physical parameters, while the second enables us to study the accuracy of Spoc's photometric redshifts.

Table 2 compares the means and 95% confidence intervals for the various physical parameters of each galaxy that result from the various models, while Figure 9 shows the 68 and 99% contours in the  $M^*-\text{SFR}$  space for the same models. While fitting with toy models, we confirmed that the probability density varies only weakly with  $Z$  (Papovich et al. 2001); for this reason we have omitted  $Z$  from Table 2. Our simulations, combined with Spoc, suggest that all of the objects have  $0.1 \leq Z \leq 0.3$  (Davé et al. 2006).

Figure 8 compares the synthetic spectra of the best-fit  $j_{\text{yzw}}$  models with the published rest-frame UV through optical data for our sample. Table 2 shows that we obtain very good fits ( $\chi^2 \approx 2$ ) with the simulated library in all cases except for the unusual object GLARE # 3001. Note that these spectra and  $\chi^2$  values are purely representative; in practice we obtain physical constraints through the Bayesian analysis described in Section 2 rather than by simply examining the best-fitting model. It is encouraging that the fits obtained from our simulated galaxy library are generally equally as compelling, in terms of  $\chi^2$ , as the fits that result from the toy model libraries. Evidently  $\chi^2$  by itself cannot reveal much

about the SFH of an observed galaxy given the present measurements.

Taken together, these findings strongly support the possibility that most observed reionization-epoch galaxies possess theoretical analogues within our simulations, and that we can use such simulations to constrain their physical properties. However, some of these objects show minor discrepancies that may be hinting at some failing in the models. Given the currently large observational uncertainties it is difficult to place robust constraints on the models, but it is nevertheless worthwhile to discuss each of these systems in detail in order to illustrate how Spoc can be used to both reveal physical characteristics as well as test the underlying model.

**A370 HCM 6A:** We have taken the photometric data and errors in the observed  $R, Z, J, H, K'$ , and Spitzer/IRAC bands from Chary, Stern & Eisenhardt (2005, hereafter CSE05), and we have adopted their lensing magnification factor of 4.5. The measured 4.5 m flux is anomalously large; CSE05 interpret the excess over the inferred stellar continuum as H emission line flux and derive an SFR of  $140 \pm 90 \text{ M}_\odot \text{ yr}^{-1}$ . In our simulations galaxies at  $z = 6.5$  that possess this object's 3.6 m flux are forming stars at  $2 \pm 12 \text{ M}_\odot \text{ yr}^{-1}$ . Since such systems are not expected to produce H equivalent widths that would contribute significantly to the broadband flux, we adopt the uncorrected 4.5 m measurement. We verified that, if we use the H-corrected 4.5 m flux obtained by CSE05, the inferred SFR drops from  $6.1 \pm 2.3$  to  $4.9 \pm 1.9 \text{ M}_\odot \text{ yr}^{-1}$ ; this value is in conflict with the assumed line strength as expected. The 8.0 m limits quoted in the text of CSE05 are different from the limit plotted in their Figure 2; we adopt the less restrictive limit from the Figure.

When we do not enforce the spectroscopic redshift, the photometric redshift  $5.9 \pm 0.4$  is dominated by the  $R-Z$  limit and is roughly 1.5 below the spectroscopic redshift; the formal redshift uncertainty is dominated by the size of the  $R-Z$  baseline. Although the toy models yield more accurate photometric redshifts in this case, the difference is comparable to the formal uncertainty and we regard it more as a coincidence than as a clue to the SFH of this object. A more accurate photometric redshift would require us to include the unpublished measurement in  $I$  and an accurate  $Z^0$  transmission curve; we have used the SDSS  $z^0$  profile because a transmission curve for the  $Z^0$  measurement used by Hu et al. (2002) is not available.

The fits that we obtain are very good, although we confirm that the 4.5 m measurement is difficult to interpret as purely stellar continuum emission. In fact, even without the anomalous 4.5 m flux the UV continuum is difficult to understand owing to the dip at  $K^0$  (Schaerer & Pello 2005), and the measured Ly flux is difficult to reconcile with the observed Ly luminosity function at  $z = 6.5$  (Malhotra & Rhoads 2004; Kashikawa et al. 2006). Thus, until more precise measurements of this object are available, any inferences regarding its physical properties should probably be regarded as suggestive.

With these caveats in mind, we find that using the simulated models yields inferred stellar mass, SFR, and  $A_V$  that are fully consistent with previous derivations as well as with the toy model SFHs. The range of stellar masses allowed by the  $j_{\text{yzw}}$  models nicely brackets the range between the emission-line-dominated and stellar-continuum-dominated solutions.

tions suggested by CSE 05, and the range of SFRs is consistent with the derivation of Hu et al. (2002) based on the Ly line and well below the inferred H-based SFR of CSE 05. Turning to the toy models, the widest uncertainties for all of the parameters are provided by the decaying model, with the results from the constant and rising models spanning a somewhat smaller subset of this space. The results from the rising model are generally the closest match to the JVZW models although they permit a somewhat larger range of SFR; these are burst-like models that have no analogue in our simulations.

**SBM 03# 1, SBM 03# 3, GLARE# 3001:** We adopted the measured broadband fluxes and spectroscopic redshifts for these objects from Tables 1 and 2 in Eyles et al. (2005). Object SBM 03# 1 is the same as object # 1ab in Yan et al. (2005). Comparing the derived fluxes in these two papers, we find disagreement at the 1 level in the ACS  $\lambda_{455}$ ,  $z_{850}$ , and NICMOS  $H_{160}$  bands. To be conservative, we therefore impose a minimum uncertainty of 0.15 mag in all bands for these objects. When fitting for the photometric redshifts we include the  $i_{775}$  fluxes; otherwise we exclude this datum following Eyles et al. (2005). Figure 8 shows that we obtain an excellent fit for SBM 03# 1 and satisfactory fits for SBM 03# 3 and GLARE# 3001, with the chief difficulty in the latter objects being the anomalous fluxes in  $K_S$  as noted by Eyles et al. (2005).

For objects SBM 03# 1 (Dickinson et al. 2004; Stanway et al. 2004a, 2003) and SBM 03# 3 (Bunker et al. 2003; Stanway et al. 2003) Spoc deduces stellar masses of  $10^{10} M_{\odot}$  and mean ages that include the range 100–300 Myr irrespective of the assumed SFH, consistent with the findings of Eyles et al. (2005). The minimum age for each model is older than the ages for the other objects in our sample because the small measured uncertainties on the 3.6  $\mu$ m fluxes for SBM 03# 1 and # 3 create the strongest case for a pronounced Balmer break. In our simulations, such objects are roughly 130–200 Myr old and are forming stars at a healthy  $30(60) M_{\odot} \text{ yr}^{-1}$  (both 1). The resulting intrinsically blue colours cause Spoc to select moderate dust extinctions  $A_V$  of 0.4–0.9 and 0–0.1 for # 1 and # 3, respectively, in order to match their UV continuum slopes. While these SFRs are within the full range inferred via the toy models, they are generally more active and younger than inferred via the decaying and constant models. The discrepancy owes primarily to the fact that the constant and decaying models permit higher SFRs at early times ( $z < 10$ ) than occur in our simulations. Because the rising model excludes such early episodes, it yields constraints that are more similar to the results from the JVZW models.

The photometric redshifts for SBM 03# 1 and # 3 are 1–3 below the spectroscopic values for both simulation and toy models, suggesting that unknown systematic uncertainties such as uncertainty owing to inaccurate iterates should be folded into the formal uncertainties; in future work an enforced minimum redshift uncertainty of  $z = (1+z) > 0.02$  seems reasonable.

Object GLARE# 3001 is a particularly interesting case because it represents the worst fit for all our models. This object shows a relatively flat SED with little evidence for a Balmer break (Figure 8). The photometric redshifts are systematically high although they are accurate at the 1 level. Spoc finds that it is perhaps an order of magnitude

less massive than SBM 03# 1 and # 3. In our simulations, the analogues to GLARE# 3001 are of roughly the same age as the SBM objects while their SFRs are roughly one tenth as large, leading to similarly strong Balmer breaks and dust extinctions. Comparing with the toy model SFHs, Table 2 shows that, for this object, constant and rising models yield masses, SFRs, and ages that are marginally consistent with the results from our simulations (although they are skewed to higher SFR) while decaying models yield extremely young, burst-like fits whose parameters are entirely inconsistent with the JVZW results (this is especially clear in Figure 9).

The chief difficulty in fitting GLARE# 3001 is the anomalously high flux measured in  $K_S$ , as noted by Eyles et al. (2005). If real, this would suggest that this is a low-mass object undergoing a burst. Table 2 shows that the  $\chi^2$  per degree of freedom is lower for the toy models than for the simulated models, because the toy models have the freedom to produce a higher  $K_S$  flux through a higher SFR and  $A_V$  together with a lower stellar mass; galaxies with these combinations of high SFR ( $> 10 M_{\odot} \text{ yr}^{-1}$ ) and low stellar mass ( $< 10^9 M_{\odot}$ ) simply do not occur in our simulations. It would be preliminary to stake the final interpretation of this galaxy on one broadband measurement (particularly one in  $K_S$ ), especially since even the toy model fits are not particularly good (2 & 3). But this object does illustrate how Spoc can pick out galaxies that may provide the most stringent tests of galaxy formation models.

**Y05# 5abc, # 7ab:** We adopted the Hubble/ACS+NICMOS and Spitzer/IRAC fluxes for objects # 5abc and # 7ab from the  $z < 6$  sample in Yan et al. (2005) and imposed a minimum uncertainty of 0.15 mag in all bands as before. Spoc failed to find an acceptable fit for object # 5abc, for either simulated or toy model SFHs. This object is evidently a blend of at least three components located at different redshifts and should therefore be fit with multiple components (Yan et al. 2005); however, this is beyond the scope of the present work. We therefore do not show the results from # 5abc.

By contrast, we obtain excellent fits for object # 7ab. This is somewhat surprising given that # 7ab is clearly a mixture of two components (Figure 1 in Yan et al. (2005)), and probably owes largely to the fact that it does not show anomalous single-band fluxes in the way that HCM 6A, SBM 03# 3, and GLARE# 3001 do. The photometric redshift is constrained to  $6.2 \pm 0.2, 1.5$  higher than the photometric redshift determined by Yan et al. (2005) (although they do not quote an uncertainty). Stellar mass is relatively poorly constrained owing to the relatively low signal-to-noise in the observed 3.6  $\mu$ m band. As Figure 9 shows, when we apply Spoc with our simulated models, the poorly-constrained stellar mass leads directly to a poorly-constrained SFR. Comparing with the toy models, we find that these span an even larger (overlapping) space. This object illustrates the importance of high-quality near-infrared data in order to understand the physical properties of high-redshift galaxies.

Yan et al. (2005) applied exponentially-decaying models to this object and found a burst-like best-fit solution with a stellar mass of  $\log(M/M_{\odot}) = 9.5$  (when converted to a Chabrier IMF), little current star formation ( $< 0.001 M_{\odot} \text{ yr}^{-1}$ ), no dust extinction, and an age of 50–

100 M yr. The stellar mass is fully consistent with our jzw results. However, we find disagreement in the inferred dust extinction, SFR, and age because in the simulations galaxies of this stellar mass and redshift are invariably older and are still forming stars. In particular, we expect  $A_V = 0.34 \pm 0.24$ ,  $M_* = 9.5 M_\odot$  yr $^{-1}$ , and age = 175–30 M yr (1 uncertainty). Once again, the absence of burst-like models in our simulations constitutes an effective prior that excludes such solutions. When we apply our own exponentially-decaying models to this object we find that the probability density possesses a sharp peak at low ages (< 100 M yr) and a broad but slightly lower plateau at older ages. So while we formally obtain the lowest  $\chi^2$  for burst-like models, folding in our simulation prior leads to an older age being preferred. This object is therefore a classic case where simply taking the lowest  $\chi^2$  among all SFHs results in a substantially different interpretation than that obtained using physically-motivated priors. It will be interesting to see with improved observations whether or not the simulation prediction ends up being correct.

In these fits, we have not considered the possibility of any AGN contribution to the SEDs. From rest-UV photometry alone it is difficult to rule out this possibility. Fitting power laws of the form  $f \propto z^{\alpha}$  to their rest-frame UV continua, we obtain slopes in the range  $-2 \leq \alpha \leq 1.1$  with a weighted mean of -0.61. These are not significantly different from the slopes inferred by Fan et al. (2001) from 39 quasars at  $3.66 \leq z \leq 4.77$ , with a mean and standard deviation of -0.79 and 0.34, respectively. However, with Spitzer/IRAC photometry the Balmer breaks in Abell 2218 KESR, SBM 03# 1, SBM 03# 3, and Y05# 7ab are clearly evident. Furthermore, Stanway et al. (2004a) and Bunker et al. (2003) argue that AGN can be ruled out for three of the objects (SBM 03# 1, SBM 03# 3, and GLARE# 3001) based on upper limits to the flux of the N V doublet at 1240Å, the lack of any X-ray detection, and the relatively small velocity width of the observed Lyman lines ( $v_{FWHM} < 500$  km s $^{-1}$ ). These arguments also apply to Abell 2218 HCM 6A. Additionally, CSE05 note that the latter object is similar to high-redshift Lyman emitters, for which the AGN fraction is constrained to be less than 5% (e.g., Gawiser et al. 2006; Ouchi et al. 2005; Dawson et al. 2004; Wang et al. 2004; Santos et al. 2004). This suggests that AGN do not dominate their rest-frame optical spectra, and emphasizes the usefulness of Spitzer/IRAC measurements for constraining the properties of reionization-epoch objects. Hence it seems reasonable to model all of these objects with stellar population synthesis models alone, as we have done.

In summary, we are usually able to find galaxies within our simulations whose synthetic photometry suggests that they could be the theoretical counterpart to observed reionization-epoch galaxies. Using these models as inputs to our SED-fitting engine, Spoc, we obtain physical constraints on the properties of the galaxies that are, in five out of six cases, consistent with the results from one-parameter SFHs. In the remaining case, the observed SED leads the toy models to prefer burst-like scenarios that do not occur in our simulations. In all cases the tightness of constraints from the simulated models is equal to or better than that from toy model SFHs. Albeit small, this sample of systems illustrates how using Spoc to compare among SFHs can provide insights into the physics of early galaxy formation, and iden-

tify unusual galaxies that provide the tightest constraints on such models.

## 7 SUMMARY AND CONCLUSIONS

The central message from this paper is that, individually, observed reionization-epoch galaxies are generally reproduced within the current generation of galaxy formation simulations, and further that it is possible to use such simulations to more tightly constrain the physical properties of observed galaxies. To this end, we have developed a code called Spoc capable of deriving the intrinsic physical properties of high-redshift galaxies by optimally comparing their broadband measurements with synthetic photometry from numerically-simulated model galaxies via a Bayesian engine.

We have verified that the technique self-consistently recovers the intrinsic physical properties of a test set of simulated galaxies. By comparing the inferred and correct values we have found that the scatter in the resulting errors is comparable to or less than the formal 1-uncertainty, with both smaller than 40% for all of the properties that we have considered. By repeating this experiment with constant, decaying, and rising SFHs, we have found that the toy models perform noticeably worse. In particular, we find that using toy models results in large systematic errors particularly in the inferred star formation rate, with the decaying models yielding the largest discrepancies. Redshift is more accurately recovered at  $z = (1+z) < 1\%$  although, once again, the numerical models show the smallest systematic offset at 0.2%.

Using Abell 2218 KESR we demonstrated that all of the best-fit parameters except metallicity are insensitive to the explored choices for superwind feedback model, dust extinction model, and cosmology. While this is disappointing for attempts to distinguish between such wind models based on these galaxies, it lends substantial robustness to the inferred physical properties. The choice of dust prescription also makes little difference for any physical property except (unsurprisingly)  $A_V$ , although redshift can be affected at the 1% level.

In order to explore the variety of interpretations from high-redshift galaxy observations, we have used Spoc to locate potential theoretical analogues to two likely and four confirmed  $z > 5.5$  objects from the literature. We have shown that fits obtained from numerically-simulated models are broadly equivalent (in terms of  $\chi^2$ ) to the fits that result from various toy model SFHs. However, because the range of simulated SFHs is a small subset of the full range of physically plausible SFHs, using the simulated models results in implicit priors on the inferred intrinsic physical properties, leading to tighter formal uncertainties. We argue that, because our simulations are able to reproduce a wide range of observations of the high-redshift universe, these tighter constraints are not only more precise, they are also likely more accurate.

In this work we have performed the simplest possible spectral synthesis calculations, primarily because our focus has been a comparison between different SFH models. However, more work is clearly needed in order to investigate different population synthesis models (e.g., Maraston et al. 2006), IMFs (e.g. Fardal et al. 2006), and nonstellar contri-

butions to the observed fluxes such as emission lines from H II regions.

In the future, we hope to apply Spoc to a larger sample of galaxies. This would enable a number of interesting investigations. First, the bulk statistics (e.g. stellar mass or star formation rate functions) produced by Spoc using simulated galaxies can be compared against that directly produced in simulations. While this is partly a circular comparison because simulated galaxies are being used to infer the physical properties, in practice there is no guarantee that consistency will be achieved because the simulated SFHs are quite generic; hence this should provide a stringent test of models of galaxy formation. Second, Spoc can be used to identify populations of galaxies that deviate dramatically from simulation predictions, in order to isolate which physical processes may be missing in models. In principle this can quantify the contributions from nonstellar emission-dominated sources such as AGN and extremely dusty objects. Finally, the redshift evolution of the galaxy population provides a strong test of models, particularly investigating the dramatic change in the nature of massive galaxies that appears to occur at  $z \approx 1-2$  (Kopovich et al. 2005).

Spoc is a general-purpose code, in principle able to utilize any type of model that produces detailed galaxy SFHs, be it a hydrodynamic, semi-analytic, or analytic model. There is nothing in principle that limits it to high redshift, with the exception of the believability of the input model spectra. We are currently planning to make Spoc and our latest library of simulated galaxies publicly available in summer 2007. We hope that Spoc will be a useful and flexible tool for conducting detailed comparisons between simulations and observations, as are critical for advancing our understanding of galaxy formation.

#### ACKNOWLEDGEMENTS

We thank C. Papovich for a great deal of encouragement and an inexhaustible stream of useful suggestions. We also thank D. Zaritsky, E. Egami, and R. Thompson for helpful conversations, and V. Springel and L. Hernquist for providing us with Gadget-2. The simulations were run in part on the Xeon Linux Supercluster at the National Center for Supercomputing Applications, along with a 100-processor cluster here at Steward Observatory. KMF acknowledges support from a National Science Foundation Graduate Research Fellowship. Support for this work was also provided by NASA through grant number HST-AR-10647 from the Space Telescope Science Institute, which is operated by the Association of Universities for Research in Astronomy, Inc., under NASA contract NAS-26555. Support for this work, part of the Spitzer Space Telescope Theoretical Research Program, was further provided by NASA through a contract issued by the Jet Propulsion Laboratory, California Institute of Technology under a contract with NASA.

Table 1. Derived Parameters for Abell 2218 KESR

M odel <sup>a</sup>	A <sub>V</sub> <sup>b</sup>	Z <sup>c</sup>	Age (M yr)	M— <sup>d</sup> (M yr <sup>-1</sup> )	log(M =M ) <sup>d</sup>	z		
nw	0.21	0.14	0.0041	0.0007	147 30	2.2 0.6	8.71 0.13	6.71 0.06
cw	0.14	0.12	0.0035	0.0005	160 33	2.0 0.6	8.73 0.14	6.71 0.06
vzw	0.17	0.12	0.0018	0.0002	175 25	2.2 0.6	8.78 0.12	6.71 0.06
jzwm	0.23	0.13	0.0020	0.0002	160 12	2.4 0.7	8.74 0.12	6.71 0.06
Egami et al. (2005)				50{450		0.1{3.3	8.5{8.8	6.6{6.8
Schaerer & Pello (2005)	0.2			3{400		1.5{1.9	7.7{9.0	6.0{7.2

<sup>a</sup>nw, cw, vzw denote no, constant and momentum-driven winds, respectively; jzwm uses 3rd-year WMAP cosmology.

<sup>b</sup>Assumes the Calzetti et al. (2000) dust prescription and R<sub>V</sub> = 4.05.

<sup>c</sup>metal mass fraction in stars

<sup>d</sup>Assumes a Chabrier IMF. To convert from a Chabrier IMF to a Salpeter IMF from 0.1{100 M<sub>sun</sub>, multiply by 1.5.

Table 2. Mean and 2<sup>nd</sup> Parameter Ranges for z > 5.5 Galaxies

Name	M odel <sup>a</sup>	A <sub>V</sub> <sup>b</sup>	Age/M yr	M— <sup>c</sup> (M yr <sup>-1</sup> )	log(M =M ) <sup>c</sup>	z <sup>d</sup>	z <sup>e</sup>
A 2218 KESR	jzwm	0.23 (0{0.53)	160 (132{181)	2.4 (1.2{3.7)	8.7 (8.5{9.0)	6.71 0.06	0.57
	constant	0.42 (0{1.0)	107 (7{350)	6.7 (2{25)	8.7 (8.1{9.1)	6.68 0.08	0.62
	decaying	0.34 (0{1.00)	104 (8{370)	6.9 (1.0{25.2)	8.7 (8.1{9.1)	6.68 0.07	0.55
	rising	0.33 (0{0.87)	129 (5{268)	3.5 (1.5{12.5)	8.7 (8.2{9.1)	6.69 0.07	0.60
A 370 HCM # 6A	jzwm	0.49 (0{1.08)	191 (122{250)	7.8 (2.7{18.2)	9.3 (8.9{9.6)	6.56=5.87	0.35 1.7
	constant	0.76 (0.13{1.24)	182 (24{402)	14.0 (4.1{28.1)	9.6 (9.0{9.9)	6.56=6.18	0.41 1.5
	decaying	0.55 (0{1.37)	217 (9{502)	16.4 (0.6{83.5)	9.5 (8.7{9.9)	6.56=6.15	0.41 1.5
	rising	0.82 (0.13{1.37)	138 (8{282)	16.1 (4.2{40.1)	9.4 (8.8{9.8)	6.56=6.15	0.41 1.6
SBM 03# 1	jzwm	0.67 (0.36{0.93)	175 (123{231)	42.1 (30.9{62.1)	10.1 (9.9{10.2)	5.83=5.64	0.08 1.7
	constant	0.45 (0.25{0.62)	388 (235{498)	24.5 (18.0{29.3)	10.2 (10.1{10.4)	5.83=5.68	0.08 1.2
	decaying	0.29 (0{0.75)	357 (89{601)	20.7 (0.63{99.6)	10.3 (10.0{10.5)	5.83=5.68	0.08 0.9
	rising	0.78 (0.50{1.12)	212 (51{332)	51.7 (29.5{102.0)	10.2 (10.0{10.4)	5.83=5.65	0.08 1.6
SBM 03# 3	jzwm	0.44 (0.09{0.69)	170 (124{231)	46.1 (24.9{75.3)	10.1 (9.9{10.3)	5.78=5.68	0.07 2.2
	constant	0.18 (0{0.37)	385 (225{498)	25.0 (18.0{29.3)	10.3 (10.0{10.4)	5.78=5.74	0.07 1.7
	decaying	0.25 (0{0.87)	301 (30{601)	41.9 (8.3{251.0)	10.3 (9.9{10.6)	5.78=5.71	0.08 1.5
	rising	0.58 (0.25{1.00)	188 (25{332)	64.9 (28.4{159.2)	10.2 (9.9{10.4)	5.78=5.69	0.08 2.0
GLARE # 3001	jzwm	0.19 (0{0.46)	183 (123{253)	5.2 (3.4{8.7)	9.2 (9.0{9.3)	5.79=5.86	0.07 8.7
	constant	0.47 (0.12{0.62)	31 (6{126)	18.9 (6.2{29.3)	8.8 (8.4{9.2)	5.79=5.81	0.07 3.5
	decaying	0.59 (0.13{0.87)	15 (6{85)	30.3 (7.4{63.3)	8.7 (8.4{9.2)	5.79=5.80	0.08 3.3
	rising	0.53 (0{0.87)	42 (5{200)	17.6 (5.1{40.1)	8.8 (8.4{9.3)	5.79=5.81	0.08 3.0
Y 05# 7ab	jzwm	0.34 (0{0.94)	175 (126{227)	9.2 (3.7{26.7)	9.4 (9.0{9.8)	6.25 0.16	0.56
	constant	0.56 (0{1.00)	210 (27{448)	16.2 (4.7{28.7)	9.7 (8.8{10.3)	6.17 0.17	0.18
	decaying	0.48 (0{1.24)	212 (10{532)	22.7 (0.8{105.3)	9.7 (8.5{10.4)	6.15 0.18	0.14
	rising	0.63 (0{1.37)	140 (5{299)	20.3 (4.6{63.8)	9.5 (8.7{10.2)	6.18 0.18	0.35

<sup>a</sup>"jzwm" denotes the simulated galaxies; "constant", "decaying", and "rising" denote representative one-parameter SFH models.

<sup>b</sup>Assumes the Calzetti et al. (2000) dust prescription and R<sub>V</sub> = 4.05.

<sup>c</sup>Assumes a Chabrier IMF. To convert from a Chabrier IMF to a Salpeter IMF from 0.1{100 M<sub>sun</sub>, multiply by 1.5.

<sup>d</sup>Where 2 numbers are given, the first is the spectroscopic redshift and the second is the photometric redshift.

<sup>e</sup>M <sub>minim</sub> reduced <sup>2</sup> for each combination of models and observed object. The number of degrees of freedom is given by the number of detections used minus 3 for A 2218 KESR and Y 05# 7ab, and minus 2 for the others.

## REFERENCES

Ajiki, M., Mobasher, B., Taniguchi, Y., Shioya, Y., Nagao, T., Murayama, T., & Sasaki, S. S. 2006, *ApJ*, 638, 596

Balogh, M. L., Pearce, F. R., Bower, R. G., & Kay, S. T. 2001, *MNRAS*, 326, 1228

Benitez, N. 2000, *ApJ*, 536, 571

Berger, E. et al., *ApJ*, submitted, [astro-ph/0603689](#)

Bouwens, R. J., Thompson, R. I., Illingworth, G. D., Franx, M., van Dokkum, P. G., Fan, X., Dickinson, M. E., Eisenstein, D. J., Rieke, M. J. 2004, *ApJ*, 616, L79

Bouwens, R. J., et al. 2004, *ApJL*, 606, L25

Bouwens, R. J., Illingworth, G. D., Blakeslee, J. P., & Franx, M. 2006, *ApJ*, in press, [astro-ph/0509641](#)

Bruzual, G. & Charlot, S. 2003, *MNRAS*, 344, 1000

Bunker, A. J., Stanway, E. R., Ellis, R. S., McMahon, R. G., & McCarthy, P. J. 2003, *MNRAS*, 342, L47

Calzetti, D., Armus, L., Bohlin, R. C., Kinney, A. K., Koomneef, J., & Storchi-Bergmann, T. 2000, *ApJ*, 533, 682

Cardelli, J. A., Clayton, G. C., & Mathis, J. S. 1989, *ApJ*, 345, 245

Charlot, S., & Fall, S. M. 2000, *ApJ*, 539, 718

Chary, R.-R., Stern, D., & Eisenhardt, P. 2005, *ApJL*, 635, L5 (CSE05)

Cuby, J.-G., Le Fèvre, O., McCracken, H., Cuillandre, J.-C., Magnier, E., & Méneux, B. 2003, *A&A*, 405, L19

Davé, R., Finlator, K., & Oppenheimer, B. 2006, *MNRAS*, accepted, [astro-ph/0511532](#)

Dawson, S., et al. 2004, *ApJ*, 617, 707

Dickinson, M., et al. 2004, *ApJL*, 600, L99

Ditory, N., Salvato, M., Gabasch, A., Bender, R., Hopp, U., Feulner, G., & Pannella, M. 2005, *ApJL*, 619, L131

Dunlop, J. S., Cirasuolo, M., & McLure, R. J., *MNRAS*, submitted, [astro-ph/0606192](#)

Erb, D. et al. 2006, *ApJ*, accepted, [astro-ph/0604041](#)

Egami, E. et al. 2005, *ApJ*, 618, L5

Eyles, L. P., Bunker, A. J., Stanway, E. R., Lacy, M., Ellis, R. S., & Doherty, M. 2005, *MNRAS*, 364, 443

Fan, X., et al. 2001, *AJ*, 121, 31

Fardal, M., Katz, N., Weinberg, D., & Davé, R. 2006, *MNRAS*, submitted, [astro-ph/0604534](#)

Finlator, K., Davé, R., Papovich, C., & Hemquist, L. 2006, *ApJ*, 639, 672

Gawiser, E., et al. 2006, *ApJL*, 642, L13

González-Serrano, J. I., Cepa, J., Pérez-García, A. M., Gallego, J., Alfaro, E. J., Sanchez-Portal, M., & González, J. J. 2005, *Revista Mexicana de Astronomía y Astronómica Conference Series*, 24, 247

Gordon, K. D., Clayton, G. C., Misselt, K. A., Landolt, A. U., & Wolf, M. J. 2003, *ApJ*, 594, 279

Gwyn, S. D. J., & Hartwick, F. D. A. 2005, *AJ*, 130, 1337

Haardt, F. & Madau, P. 2001, in proc. XXXV Ith Rencontres de Moriond, eds. D. M. Neumann & J. T. T. Van.

Hu, E. M., Cowie, L. L., McMahon, R. G., Capak, P., Iwamuro, F., Neib, J.-P., Mihara, T., & M. Otohara, K. 2002, *ApJL*, 576, L99

Hu, E. M., Cowie, L. L., Capak, P., McMahon, R. G., Hayashino, T., & Komiyama, Y. 2004, *AJ*, 127, 563

Iben, I. J. 1967, *ARA&A*, 5, 571

Idzi, R., Somerville, R., Papovich, C., Ferguson, H. C., Giavalisco, M., Kretchmer, C., & Lotz, J. 2004, *ApJL*, 600, L115

Kashikawa, N., et al. 2006, [astro-ph/0604149](#)

Kaumann, G., et al. 2003, *MNRAS*, 341, 33

Kawai, N., et al. 2006, *Nature*, 440, 184

Kennicutt, R. C. 1998, *ApJ*, 498, 541

Keres, D., Katz, N., Weinberg, D. H., & Davé, R. 2005, *MNRAS*, in press

Keel, J.-P., Ellis, R. S., Santos, M. R., & Richard, J. 2004, *ApJL*, 568, L75

Kodaira, K., et al. 2003, *PA SJ*, 55, L17

Kurk, J. D., Camatti, A., di Serego Alighieri, S., Vernet, J., Addi, E., Ferrara, A., & Ciardi, B. 2004, *A&A*, 422, L13

Madau, P. *ApJ*, 441, 18

Malhotra, S. & Rhoads, J. 2004, *ApJ*, 617, L5

Malhotra, S., et al. 2005, *ApJ*, 626, 666

Maraston, C., et al. 2006, *ApJ*, submitted, [astro-ph/0604530](#)

Martin, C. L. 2005, *ApJ*, 621, 227

McKee, C. F. & Ostriker, J. P. 1977, *ApJ*, 218, 148

Muray, N., Quatert, E., & Thompson, T. A. 2005, *ApJ*, 618, 569

Mobasher, B. et al. 2005, *ApJ*, in press

Nagao, T., et al. 2004, *ApJL*, 613, L9

Nagao, T., et al. 2005, *ApJ*, 634, 142

Night, C., Nagamine, K., Springel, V., & Hemquist, L. 2005, *MNRAS*, accepted, [astro-ph/0503631](#)

Oppenheimer, B. D. & Davé, R. 2006, *MNRAS*, submitted, [astro-ph/0605651](#) (OD06)

Ouchi, M., et al. 2005, *ApJL*, 620, L1

Papovich, C., Dickinson, M., & Ferguson, H. C. 2001, *ApJ*, 559, 620

Papovich, C. et al. 2005, *ApJ*, submitted

Rhoads, J. E., & Malhotra, S. 2001, *ApJL*, 563, L5

Rhoads, J. E., et al. 2003, *AJ*, 125, 1006

Rhoads, J. E., et al. 2004, *ApJ*, 611, 59

Rupke, D. S., Veilleux, S., & Sanders, D. B. 2005, *ApJS*, accepted, [astro-ph/0506611](#)

Santos, M. R., Ellis, R. S., Keel, J.-P., Richard, J., Kuijen, K. 2004, *ApJ*, 606, 683

Schaerer, D., & Pello, R. 2005, *MNRAS*, 362, 1054

Shapley, A. E., Steidel, C. C., Adelberger, K. L., Dickinson, M., Giavalisco, M., & Pettini, M. 2001, *ApJ*, 562, 95

Shapley, A. E., Steidel, C. C., Erb, D. K., Reddy, N. A., Adelberger, K. L., Pettini, M., Barnaby, P., & Huang, J. 2005, *ApJ*, 626, 698

Shimasaku, K., et al. [astro-ph/0602614](#)

Smail, I., Chapman, S. C., Blain, A. W., & Ivison, R. J. 2004, *ApJ*, 616, 71

Somerville, R. S., Primack, J. R., & Faber, S. M. 2001, *MNRAS*, 320, 504

Spergel, D. N. et al., *ApJS*, 148, 175

Spergel, D. N. et al., [astro-ph/0603449](#)

Springel, V. & Hemquist, L. 2002, *MNRAS*, 333, 649

Springel, V. & Hemquist, L. 2003a, *MNRAS*, 339, 289

Springel, V. & Hemquist, L. 2003b, *MNRAS*, 339, 312

Stanway, E. R., Bunker, A. J., & McMahon, R. G. 2003, *MNRAS*, 342, 439

Stanway, E. R., et al. 2004, *ApJL*, 604, L13

Stanway, E. R., Bunker, A. J., McMahon, R. G., Ellis, R. S., Treu, T., & McCarthy, P. J. 2004, *ApJ*, 607, 704

Stem, D., Yost, S. A., Eckart, M. E., Harrison, F. A., Helfand, D. J., Djorgovski, S. G., Malhotra, S., & Rhoads, J. E. 2005, *ApJ*, 619, 12

18 **F inlator, Dave, Oppenheim er**

Stiavelli, M ., et al. 2005, *ApJL*, 622, L1  
W ang, J.X ., et al. 2004, *ApJL*, 608, L21  
W ang, J. X ., M alhotra, S ., & Rhoads, J. E . 2005, *ApJL*,  
622, L77  
W estra, E ., et al. 2005, *A & A*, 430, L21  
Y an, H ., et al. 2005, *ApJ*, 634, 109